Medicine Insights

Article

MALDI Mass Spectrometry Imaging Reveals Early, Tissue-Specific Sphingolipid Dysregulation Across the Brain-Gut-Skin Axis in a GBA1 D409V Parkinson's Disease Mouse Model

Yuexiang Zhang [1,*]

[1] Faculty of Pharmacy and Pharmaceutical Sciences, Monash University, Parkville, VIC, 3052, Australia
* Correspondence: Yuexiang Zhang, Faculty of Pharmacy and Pharmaceutical Sciences, Monash University, Parkville, VIC, 3052, Australia

Abstract: Background: Mutations in the GBA1 gene, leading to glucocerebrosidase (GCase) deficiency, are a major genetic risk factor for Parkinson's disease (PD). While systemic sphingolipid alterations are implicated, their spatial distribution in preclinical stages across central and peripheral tissues remains unclear. Methods: We employed MALDI-MSI to map sphingolipid profiles in the brain, gut, and skin of 12-week-old GBA1 D409V knock-in (KI) mice, an early-stage model of GCase deficiency. Relative lipid intensities were quantified within anatomically defined ROIs. Results: In the brain, homozygous KI mice showed significant accumulation of glucosylceramide (GlcCer) species and GM1 ganglioside specifically within the caudate putamen (CPu) compared to heterozygous mice. Along the gastrointestinal tract, GlcCer (d18:1/18:0) levels progressively increased from the duodenum to the colon, with the most profound accumulation observed in the colonic mucosa of homozygous mice. In the skin, the viable epidermis of homozygous mice exhibited significantly elevated levels of GlcCer (18:1/24:0) and a putative sulfated hexosylceramide. Conclusion: Our findings demonstrate that GCase deficiency induces early, spatially restricted, and tissue-specific sphingolipid alterations across the brain-gut-skin axis prior to overt neurodegeneration. This study establishes a spatially-anchored lipidomic framework, highlighting the colonic mucosa and epidermis as potential sites for accessible biomarker discovery in GBA1-associated parkinsonism.

Keywords: Parkinson's disease; GBA1; sphingolipid; mass spectrometry imaging; glucosylceramide; brain-gut-skin axis

Published: 10 January 2026

1. Introduction

Parkinson's disease (PD) represents the second most common neurodegenerative disorder globally, with a rapidly increasing prevalence that has led some to term it an emerging pandemic [1,2]. The disease is classically defined by a triad of motor symptoms including bradykinesia, resting tremor, and rigidity, which arise from the progressive loss of dopaminergic neurons in the substantia nigra pars compacta [3]. A critical challenge in managing PD is that by the time these motor signs become clinically apparent and a diagnosis can be made, an estimated 50-60% of these crucial neurons have already degenerated [1]. This significant diagnostic delay severely limits the efficacy of current therapeutic strategies, which primarily manage symptoms rather than halting or reversing the underlying neurodegenerative process.

Increasingly, the clinical perspective on PD has expanded to recognize a lengthy prodromal phase, which can precede motor onset by years or even decades [4]. This preclinical period is characterized by a diverse array of non-motor symptoms (NMS), including hyposmia, sleep disorders, depression, cognitive impairment, and significant gastrointestinal dysfunction, such as constipation [4,5]. The presence of these early

systemic manifestations underscores the urgent need for robust and reliable biomarkers capable of identifying individuals in the prodromal stage. The development of such biomarkers is paramount, as they would not only enable earlier diagnosis but also facilitate the testing of neuroprotective and disease-modifying therapies at a time when they are most likely to be effective before irreversible neuronal loss has occurred [1].

Genetic discoveries have provided a powerful framework for dissecting the molecular underpinnings of PD. Notably, mutations in the GBA1 gene, which encodes the lysosomal hydrolase β-glucocerebrosidase (GCase), have been identified as the most common and significant genetic risk factor for the disease [6,7]. The link between GCase dysfunction and parkinsonism is powerfully underscored by clinical observations from Gaucher disease, a lysosomal storage disorder caused by biallelic GBA1 mutations. Patients with Gaucher disease exhibit a markedly elevated lifetime risk of developing PD, and even heterozygous GBA1 carriers have a 5-to 10-fold increased susceptibility compared to non-carriers [8]. This strong dose-dependent relationship provides a clear genetic and biochemical rationale for investigating the role of this pathway in PD pathogenesis.

At the molecular level, reduced GCase activity impairs the catabolism of its primary substrate, glucosylceramide (GlcCer), leading to its accumulation within the lysosome. This initial substrate buildup triggers a cascade of downstream cellular pathologies. Sphingolipids, including GlcCer and its derivatives, are not merely inert storage molecules; they are critical structural components of cell membranes and potent signaling molecules that regulate fundamental cellular processes, including lysosomal integrity, autophagy, and immune signaling [9,10]. The accumulation of GlcCer and its deacylated form, glucosylsphingosine (GlcSph), is known to induce lysosomal dysfunction and destabilize mitochondria, creating a cellular environment conducive to neurodegeneration [11]. Crucially, a toxic bidirectional loop has been identified between GCase deficiency and α-synuclein, the protein that forms the core of Lewy bodies, the neuropathological hallmark of PD [12]. GCase deficiency promotes the aggregation of α-synuclein, while, conversely, pathological α-synuclein aggregates can further inhibit GCase activity, thus creating a self-amplifying cycle of neurotoxicity [11,12]. The resulting disruption of the broader sphingolipidome, including reported alterations in ceramides, lactosylceramides, and gangliosides, further compromises neuronal homeostasis and survival [13,14].

The pathological impact of GCase deficiency is not confined to the central ENS. PD is increasingly recognized as a systemic disorder, with pathology extending to peripheral tissues along what is now conceptualized as the brain-gut-skin axis. Gastrointestinal dysfunction is among the earliest prodromal symptoms, and evidence from both patient biopsies and animal models suggests that pathological α-synuclein aggregates can be detected in the enteric nervous system (ENS) long before they are widespread in the brain [15]. This has given rise to theories, such as Braak's hypothesis, which postulate that the pathological process may originate in the gut and spread to the brain via neuronal connections like the vagus nerve [16]. Similarly, the skin has emerged as a highly promising peripheral window into PD pathology. Aggregates of phosphorylated α-synuclein have been reliably detected in cutaneous nerve fibers from skin biopsies of PD patients, offering a potential source of accessible diagnostic biomarkers [17]. As the skin is an organ with highly active sphingolipid metabolism essential for its barrier function, it represents another key site where systemic GCase dysfunction may manifest [18,19]. The involvement of these peripheral tissues suggests that they may reflect the systemic metabolic dysregulation driving the disease and could harbor early, accessible molecular signatures of GBA1-associated pathology.

Despite growing insight into the role of sphingolipids in PD, a major methodological limitation has hindered progress. The majority of lipidomic studies have relied on bulk analytical techniques, such as liquid chromatography-tandem mass spectrometry (LC-MS/MS), performed on homogenized tissue extracts [20]. While powerful, tissue

homogenization irrevocably destroys spatial information, averaging molecular signals across diverse cell types and anatomical structures. This is a critical shortcoming, as both PD pathology and the associated lipid alterations are known to be highly heterogeneous and region-specific. For example, lipidomic changes in the human basal ganglia are pronounced, while those in cortical regions can be minimal [13]. To truly understand the origin and progression of metabolic dysfunction, spatially resolved techniques are essential to localize molecular changes within their precise anatomical context.

Matrix-assisted laser desorption/ionization mass spectrometry imaging (MALDI-MSI) is a transformative technology that overcomes this limitation. It enables the label-free, in-situ detection and visualization of hundreds of molecules, including lipids, directly from tissue sections, while preserving the underlying histological architecture [21]. By creating a molecular map of the tissue, MALDI-MSI can reveal spatial patterns of lipid distribution and abundance with cellular-level resolution. Although MALDI-MSI has been applied to study lipids in various contexts, no study to date has systematically employed this technique to investigate sphingolipid alterations across the central and peripheral tissues of a genetically defined PD model in its preclinical stage [22,23].

This study seeks to fill this critical knowledge gap by leveraging the GBA1 D409V knock-in (KI) mouse model. Unlike acute toxin-based models that often mimic late-stage pathology, this genetic model faithfully recapitulates the early and progressive lysosomal dysfunction and metabolic imbalances characteristic of the prodromal phase of GBA-associated PD, all in the absence of overt neurodegeneration [24,25]. We hypothesize that GCase deficiency in this model leads to early, tissue-specific, and spatially restricted sphingolipid alterations across the brain-gut-skin axis. Using a validated MALDI-MSI workflow, we aimed to: (1) map the spatial distribution of key sphingolipids in the brain, intestinal tract, and skin; and (2) quantitatively compare regional lipid changes across wild-type, heterozygous, and homozygous GBA1 D409V KI mice. By providing a spatially anchored readout of metabolic dysregulation, this research aims to offer novel insights into GBA1-linked disease mechanisms and identify specific anatomical niches and molecular candidates for the development of early-stage biomarkers.

2. Materials and Methods

2.1. Animal Model and Ethical Statement

All animal procedures were conducted in strict accordance with the ethical guidelines for the care and use of laboratory animals and were approved by the Florey Institutional Animal Care and Use Committee (IACUC) under protocol number 2024-022-FINMH. The study utilized male GBA1 D409V KI mice (C57BL/6N-Gba1^tm1.1Mjff/J, Strain #019106), originally sourced from The Jackson Laboratory (Bar Harbor, ME, USA) and provided by the Florey Institute of Neuroscience and Mental Health (Melbourne, VIC, Australia). These mice express the human D409V mutant GBA1 protein and carry loxP sites flanking exons 6-8, providing a well-established model for investigating GCase deficiency [25].

Animals were housed under specific pathogen-free (SPF) conditions, maintained on a 12-hour light/dark cycle, and provided with ad libitum access to standard chow and water. At 12 weeks of age, a stage representing the early, preclinical phase of metabolic dysfunction, mice were euthanized by cervical dislocation. For brain tissue analysis, group sizes were wild-type (WT; n=2), heterozygous (GBA1 D409V/+; Het; n=2), and homozygous (GBA1 D409V/D409V; Hom; n=2). For the analysis of gut and skin tissues, heterozygous mice were not included, and comparisons were made between WT (n=2) and Hom (n=2) groups.

2.2. Tissue Collection and Cryosectioning

Immediately following euthanasia, tissues were rapidly dissected, prepared for cryosectioning, and stored at -80°C until analysis.

2.2.1. Brain

Whole brains were dissected, immediately frozen on a bed of dry ice, wrapped in aluminum foil, and sealed in cryotubes with an outer parafilm layer to prevent desiccation. For imaging, brains were equilibrated to -15°C in a cryostat (Leica CM1860 UV, Leica Biosystems, Germany) and serially sectioned in the coronal plane at a thickness of 14 μm. Sections were thaw-mounted onto indium-tin oxide (ITO)-coated conductive glass slides (Bruker Daltonics, Bremen, Germany).

2.2.2. Gastrointestinal Tract

The entire gastrointestinal tract was carefully excised. Four distinct anatomical regions duodenum, jejunum, ileum, and colon were identified, separated, and rinsed with cold saline to remove contents. Each segment was flash-frozen on dry ice and stored as described for brain tissue. To minimize inter-slide variability during MALDI-MSI analysis, cryosections (14 μm thickness, -20°C) were prepared such that sections from all four gut regions of both a WT and a Hom mouse were mounted adjacent to each other on the same ITO slide.

2.2.3. Skin

Whole front paws were collected and immediately frozen on dry ice without separating the skin from the underlying muscle and bone, then stored at -80°C. The hard, keratinized tissue required a colder sectioning temperature of -32°C to obtain intact 14 μm sections, which were subsequently thaw-mounted onto ITO slides.

2.3. Sample Preparation for MALDI-MSI

Following sectioning, all slides were air-dried in a vacuum desiccator for 20 minutes to ensure complete dehydration and adherence to the slide surface.

For brain tissue sections, an additional washing step was performed to remove endogenous salts and lipids that can interfere with ionization. Sections were submerged in a 75 mM ammonium formate solution for 30 seconds, immediately removed, and air-dried again in a desiccator.

Matrix deposition was performed using an automated TM-Sprayer to ensure a uniform, homogenous microcrystalline layer. For negative-ion mode analysis of all tissues, a solution of 10 mg/mL 9-aminoacridine (9-AA, ≥98%, Sigma-Aldrich) in methanol was applied in 10 layers at a flow rate of 40μL/min. For positive-ion mode analysis of gut and skin, a solution of 10 mg/mL α-cyano-4-hydroxycinnamic acid (α-CHCA,≥99.0% HPLC grade, Sigma-Aldrich) in 70:30 acetonitrile:water (v/v) with 0.1% trifluoroacetic acid was applied under the same spray parameters. For brain tissue, positive-ion mode analysis was performed on adjacent serial sections prepared with α-CHCA. After matrix application, all slides were stored in sealed slide boxes at room temperature until MALDI-MSI analysis.

2.4. MALDI-MSI Data Acquisition

Tissue imaging was performed on a timsTOF fleX MALDI mass spectrometer (Bruker Daltonics, Bremen, Germany) equipped with a SmartBeam 3D 10 kHz laser. All tissue types were analyzed in both positive- and negative-ion modes to maximize the coverage of different sphingolipid classes.

For negative-Ion mode, sections coated with 9-AA, data were acquired in reflectron negative mode over a mass range of m/z 500-3200. A spatial resolution of 50 μm was set, with the laser firing 1000 shots per pixel at a repetition rate of 1 kHz. This mode was prioritized for detecting acidic lipids like gangliosides and sulfatides.

For positive-ion mode, sections coated with α-CHCA, data were acquired in reflectron positive mode over a mass range of m/z 300-2400. A higher spatial resolution of 20 μm was used, with 200 laser shots per pixel and a summation rate value set between

224 and 256, depending on the tissue type. This mode is optimal for detecting neutral lipids like ceramides and sphingomyelins, typically as sodium or potassium adducts.

External calibration was performed using the manufacturer's ESI-L Low Concentration Tuning Mix (Agilent Technologies, CA, USA) prior to each analytical run. Raw spectral data were collected using the flexControl software (version 3.4, Bruker Daltonics).

2.5. Post-Acquisition Histological Staining and Image Co-registration

Following MALDI-MSI data acquisition, the same tissue sections were carefully stained with Hematoxylin and Eosin (H&E) for anatomical validation. The matrix was first gently removed by washing the slides in 70% ethanol. Sections were then rehydrated in Milli-Q water, stained with Harris's hematoxylin (POCD Scientific, Australia) for 1 minute, and differentiated in 1% acid alcohol. After bluing in Scott's tap water substitute (POCD Scientific), sections were counterstained with eosin Y (POCD Scientific) for 2 minutes. Finally, the slides were dehydrated through a graded ethanol series, cleared in sulfur-free xylene (POCD Scientific), and coverslipped using DPX mounting medium (Sigma-Aldrich).

The stained slides were digitized using a widefield microscope at 50x magnification. The resulting high-resolution histological images were then imported into the SCiLS™ Lab software and co-registered with their corresponding MALDI ion images to enable precise anatomically-guided data analysis.

2.6. Data Processing and Region-of-Interest (ROI) Definition

Acquired MALDI-MSI datasets were imported into SCiLS™ Lab software (version 2025 core, Bruker Daltonics) for all subsequent processing and analysis. A standard preprocessing pipeline was applied to all datasets to reduce technical variability and enhance signal quality, which included baseline subtraction using the Top Hat algorithm and Total Ion Count (TIC) normalization to normalize for variations in signal intensity across the tissue.

Regions of interest (ROIs) were manually annotated on the co-registered H&E images. The definition of ROIs was guided by established anatomical landmarks and, where necessary, by lipid-specific ion signals that highlighted specific tissue layers.

For brain, ROIs corresponding to the caudate putamen (CPu) were delineated based on the mouse brain atlas by Paxinos and Franklin [26]. Upon inspection, a mismatch in Bregma levels was identified between the control sections (approx. Bregma +0.5 mm) and the sections from heterozygous and homozygous mice (approx. Bregma -0.94 mm). Due to the significant anatomical differences at these levels, direct quantitative comparisons between the control group and the mutant groups were deemed inappropriate for the CPu. Therefore, statistical analysis of brain tissue was restricted to the comparison between the anatomically matched heterozygous and homozygous groups.

For skin, ROIs were drawn to specifically encompass the viable epidermis, defined as the combination of the stratum basale, stratum spinosum, and stratum granulosum. Three distinct circular ROIs were annotated per sample to capture representative lipid signals from this metabolically active layer while avoiding the stratum corneum and dermis.

For gut, Given the complex and often fragile architecture of intestinal cryosections, ROIs were carefully placed in areas where the mucosal layer was histologically well-preserved and clearly visible, ensuring comparability across different samples and intestinal regions.

For quantitative comparison, the mean TIC-normalized intensity was extracted from all pixels within each defined ROI. To account for variations in the size of manually drawn ROIs, this total normalized intensity was then divided by the ROI's area in pixels, yielding a final value of mean normalized intensity per unit area for statistical analysis.

2.7. Lipid Identification and Statistical Analysis

Putative lipid identification was performed by matching the observed monoisotopic m/z values of peaks of interest to theoretical masses in the LIPID MAPS® Structure Database (LMSD) [27]. A stringent mass tolerance of ±5 ppm was applied. Annotations were made considering the ion form detected. For several key sphingolipids, preliminary annotations were further supported by tandem mass spectrometry (MS/MS) fragmentation data from unpublished work within our laboratory. A comprehensive list of annotated lipids is provided in Table 1.

Table 1. Identification of sphingolipid species detected by MALDI-MSI.

Lipid species	Observed m/z value in MALDI	Theoretical m/z	MS/MS fragments	Mass error (ppm)	Ion form
GM1(d18:1/18:0)	1544.8696	NA	Sia1A$^-$, m/z 290	6.3	[M−H]$^-$
GlcCer(d20:1/22:0)	750.4814	NA	Sphingoid base d18:1	6.3	[M−H]-
GlcCer(d20:1/20:0)	720.4397	NA	Sphingoid base d18:1	6.3	[M−H]$^-$
SM(d18:2/24:0)	835.6686	835.6663	NA	4.8	[M+Na] +
GlcCer(d18:2/22:0)	783.6738	783.6504	NA	7.7	[M+H] +
GlcCer (18:1/12:0)	666. 4847	666.4915	NA	5.9	[M+Na] +
SHexCer(t33:1)	804.4929	804.4920	NA	5.9	[M+Na] +
SM(d18:1/16:0)	725.5582	725.5568	NA	5.9	[M+Na] +
GlcCer (18:1; O3/24:0; O)	866.6690	866.6692	NA	5.9	[M+Na] +

All statistical analyses were performed using GraphPad Prism (version 10.4.1, GraphPad Software, San Diego, CA, USA) and MetaboAnalyst 6.0 [28]. For skin tissue, Principal Component Analysis (PCA) was applied to the matrix of mean normalized intensities of all detected features from the VE ROIs to visualize overall clustering patterns between genotypes. For PCA, data were median-normalized, log2-transformed, and auto-scaled. For direct comparison of individual lipid species, unpaired two-tailed Student's t-tests were used to compare heterozygous and homozygous groups or control and homozygous groups. The assumption of normality was assessed using the Shapiro-Wilk test. All data are presented as mean±standard deviation (SD). Statistical significance was defined at levels of $p < 0.05$ (*), $p < 0.01$ (**), and $p < 0.0001$ (****).

3. Results

3.1. Establishing an Anatomical Framework for Spatial Lipid Profiling

To ensure that lipid alterations were evaluated within their precise anatomical context, we established a workflow that integrated MALDI-MSI with post-acquisition histological analysis. ROIs were defined based on co-registered H&E stained images, allowing for anatomically guided quantification. In the brain, ROIs were defined to encompass the CPu, a key structure in the nigrostriatal pathway implicated in PD pathology (see Figure 1). For the skin, analysis was focused on the metabolically active viable epidermis, which was clearly delineated from the stratum corneum and dermis (see Figure 2). In the gastrointestinal tract, ROIs were carefully drawn within well-preserved regions of the mucosal layer for the duodenum, jejunum, and colon to ensure consistent sampling across the complex tissue architecture (see Figure 3). This anatomically anchored approach provided a robust framework for the subsequent comparative analysis of sphingolipid profiles.

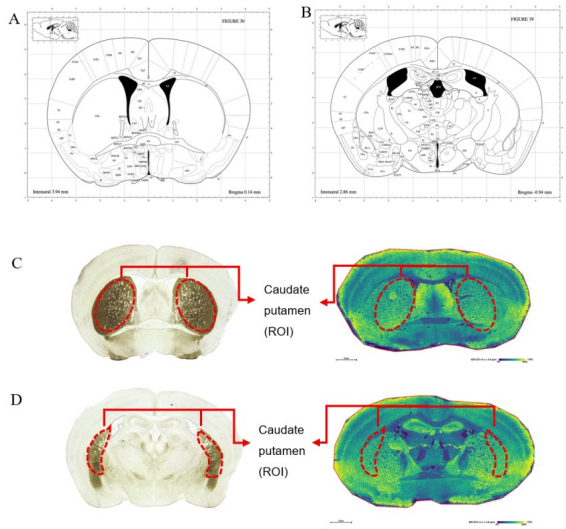

Figure 1. Definition of the CPu as the Region of Interest (ROI) in GBA1 KI Mice Brain Sections.

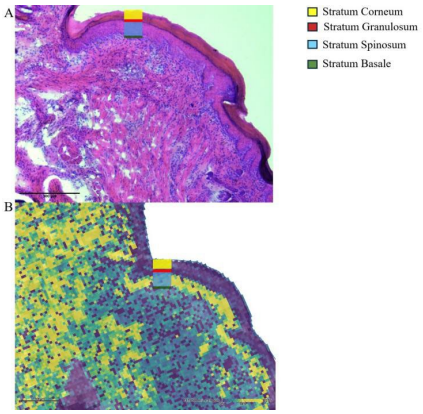

Figure 2. Definition of the Viable Epidermis as the Region of Interest (ROI) in Skin Sections of GBA1 KI Mice.

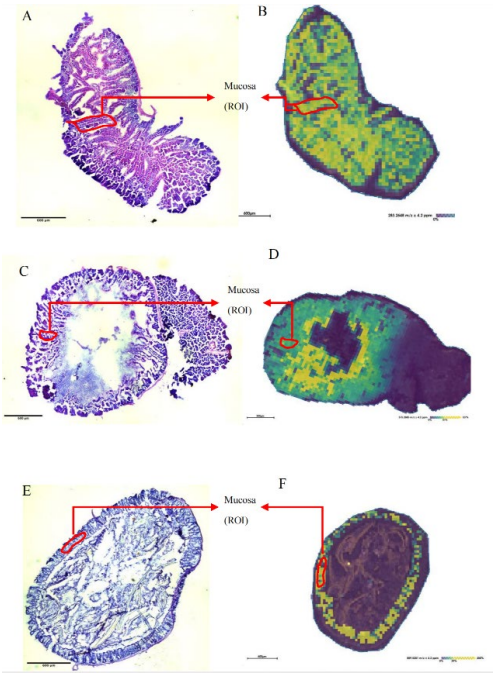

Figure 3. Definition of Mucosal ROI in Intestinal Sections of GBA1 KI Mice.

3.2. Region-Specific Accumulation of GlcCer and GM1 in the CPu of Homozygous GBA1 KI Mice

To investigate sphingolipid alterations in the central ENS, we performed MALDI-MSI on coronal brain sections. As noted in the methods, a Bregma level mismatch precluded direct quantitative comparison with the wild-type control group; therefore, statistical analysis was performed exclusively between the anatomically matched heterozygous (Het) and homozygous (Hom) GBA1 D409V KI mice.

Our analysis revealed significant, gene-dose-dependent alterations within the CPu. In the negative ion mode, the relative abundance of the ganglioside GM1(d18:1/18:0) (m/z 1544.8696) was significantly higher in the CPu of Hom mice compared to Het mice ($p < 0.01$). The corresponding ion images showed a more widespread and intense GM1 signal throughout the brain of Hom mice, with marked signal intensity in the CPu region (see Figure 4A, B).

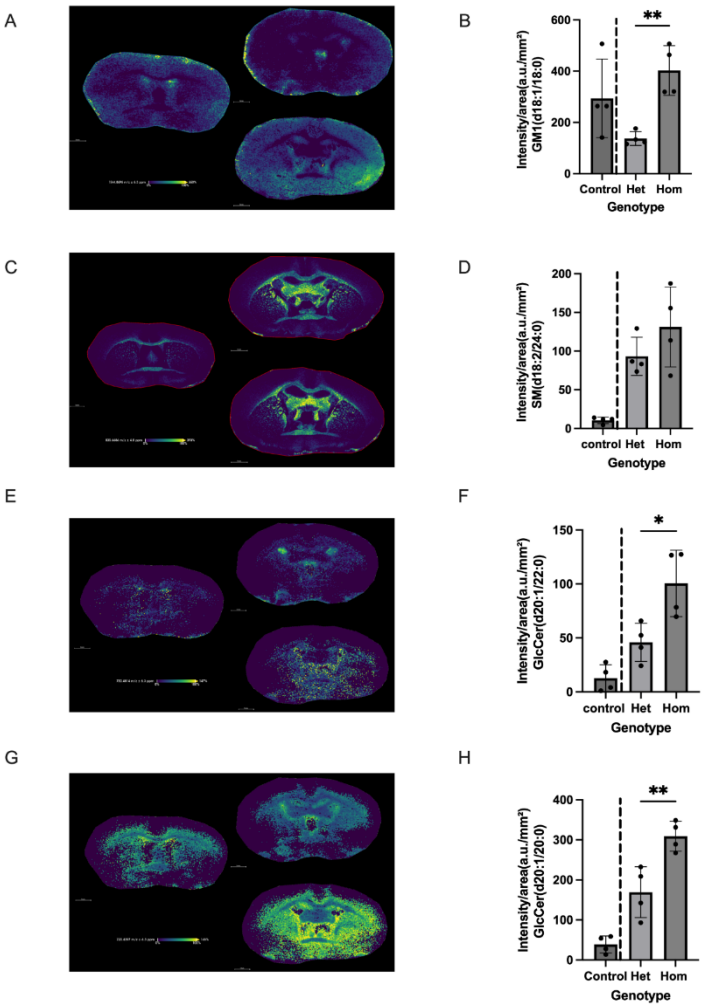

Figure 4. GM1(d18:1/18:0) (m/z 1544.8696) and GlcCer(d20:1/20:0) (m/z 750.4814) Accumulates in the CPu of homozygous GBA1 KI Mice.

Consistent with the known function of GCase, we observed a significant accumulation of its direct substrate, GlcCer. Two distinct GlcCer species, GlcCer(d20:1/22:0) (m/z 750.4814) and GlcCer(d20:1/20:0) (m/z 720.4397), were found to be significantly elevated in the CPu of Hom mice relative to Het mice ($p < 0.05$ and $p < 0.01$, respectively). The MALDI ion images visually confirmed a striking enrichment of both GlcCer species specifically within the anatomical boundaries of the CPu in the Hom

group (see Figure 4E-H). In contrast, the relative intensity of a representative sphingomyelin species, SM(d18:2/24:0) (m/z 835.6686), which is downstream of ceramide metabolism, showed no statistically significant difference between the Het and Hom groups, although a slight upward trend was observed in the Hom group (see Figure 4C, D).

3.3. Progressive GlcCer Accumulation Along the Intestinal Axis Peaks in the Colon

Given that gastrointestinal dysfunction is a prominent early feature of PD, we next investigated spatial lipid profiles along the intestinal tract. We compared sphingolipid signals in the mucosal layer of the duodenum, jejunum, and colon between Hom and WT mice.

Targeted analysis of GlcCer(d18:1/18:0) (m/z 783.6738) revealed a clear pattern of regionally heterogeneous accumulation in the Hom group. Compared to WT controls, the normalized intensity of this GlcCer was significantly elevated in the mucosa of all three intestinal segments. This increase followed a striking distal-to-proximal gradient: a significant elevation was observed in the duodenum ($p < 0.05$), which became more pronounced in the jejunum ($p < 0.01$), and culminated in a highly dramatic and significant accumulation in the colon ($p < 0.0001$) (see Figure 5).

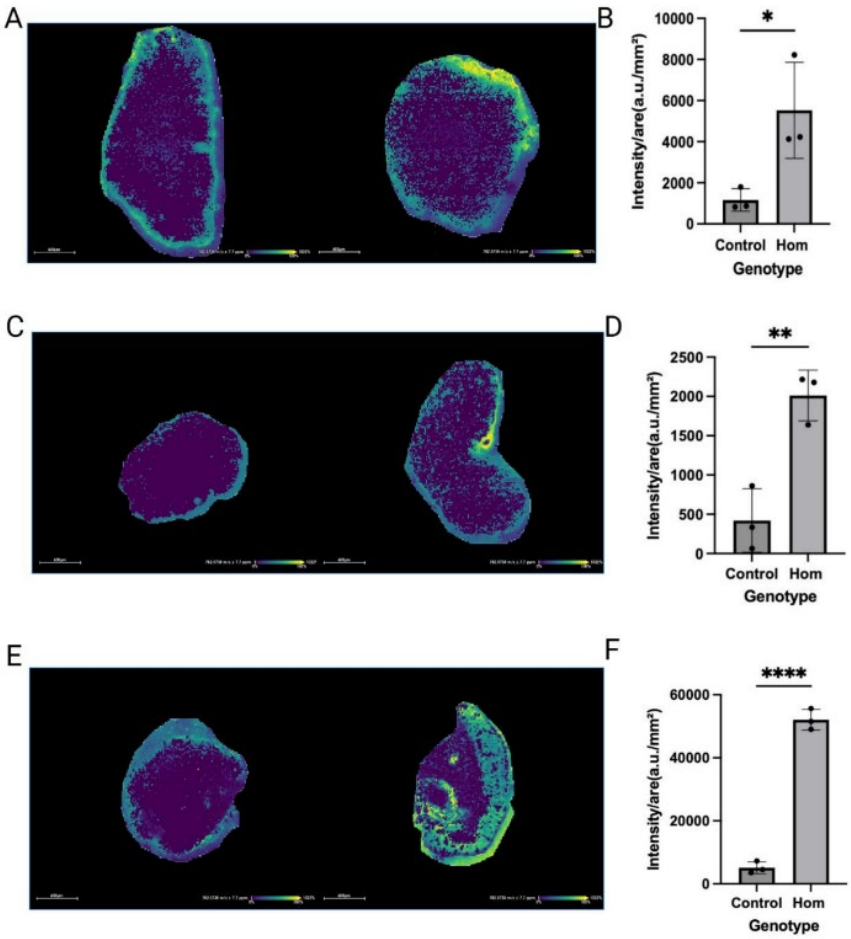

Figure 5. GlcCer (d18:1/18:0) (m/z 783.6738) Accumulation in the Intestinal Mucosa of Homozygous GBA1 KI Mice.

Furthermore, the ion distribution maps revealed segment-specific differences in the layer localization of the GlcCer signal. In the duodenum and jejunum, the signal for GlcCer(d18:1/18:0) appeared more prominent in the underlying muscularis layer. In sharp

contrast, the signal in the colon of Hom mice was intensely and preferentially localized within the mucosal layer itself. These results demonstrate that GCase deficiency leads to a spatially graded accumulation of GlcCer along the gut axis, with the colonic mucosa being the most profoundly affected region at this early disease stage.

3.4. Selective Glycosphingolipid Accumulation is Confined to the Viable Epidermis of GBA1 KI Mice

To determine if systemic GCase deficiency manifests in accessible peripheral tissues, we performed MALDI-MSI on skin sections from the paws of Hom and WT mice. A preliminary, unsupervised PCA on the full lipid dataset from the viable epidermis showed a clear and distinct clustering of the Hom group away from the WT control group, indicating a global shift in the epidermal lipid profile (see Figure 6). The first principal component (PC1) alone accounted for 44.1% of the variance between the groups. One homozygous sample was identified as an outlier and excluded from subsequent t-tests to ensure robustness of the analysis.

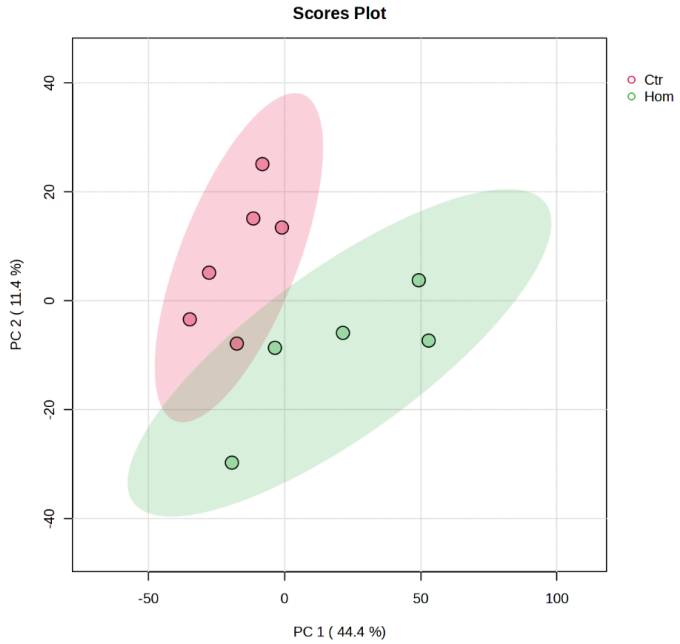

Figure 6. Positive mode PCA analysis reveals clear separation of viable epidermal (VE) lipid profiles between Control and Homozygous GBA1 KI mice.

Analysis of individual lipid species revealed that this shift was driven by the selective accumulation of specific glycosphingolipids. The relative abundance of a long-chain glucosylceramide, GlcCer(18:1/24:0) (m/z 866.6690), was significantly increased in the VE of Hom mice compared to WT controls ($p < 0.01$). Similarly, a putative sulfated hexosylceramide, SHexCer(t33:1) (m/z 804.4929), also showed significant accumulation in the Hom group ($p < 0.01$) (see Figure 7A-D).

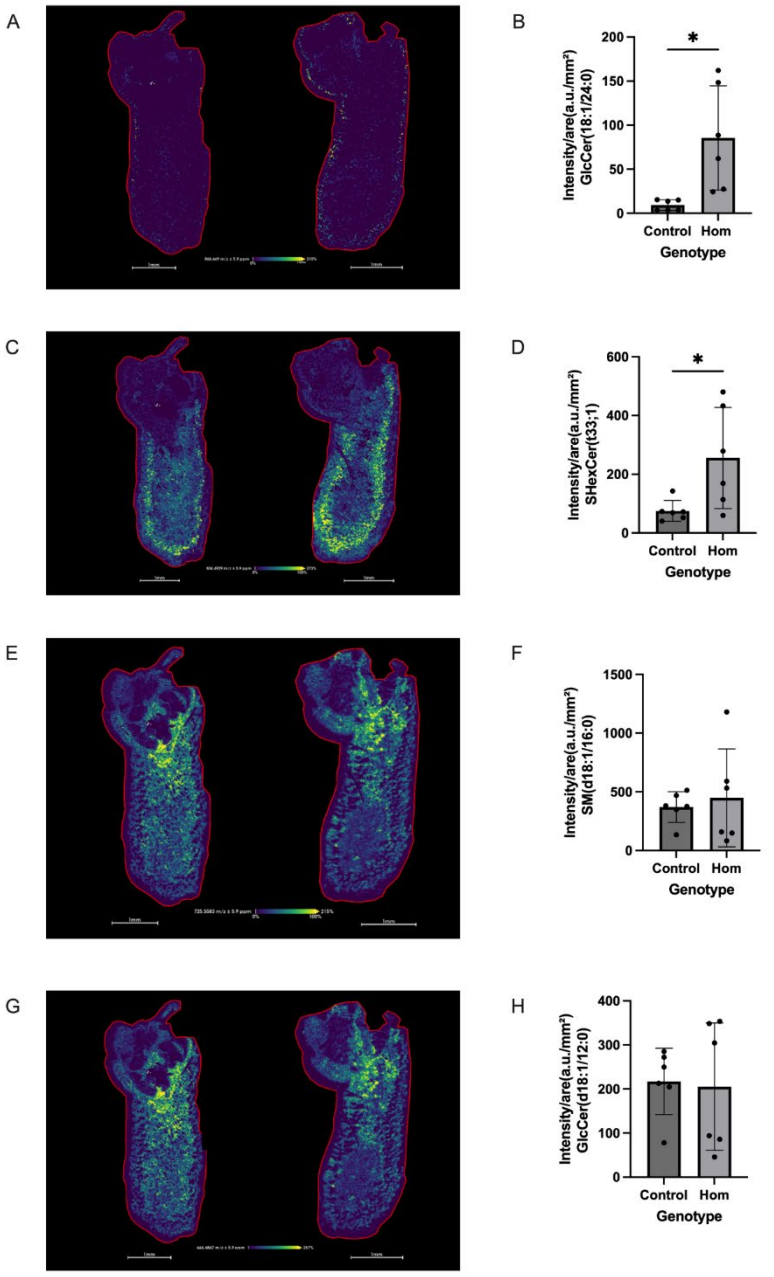

Figure 7. GlcCer (18:1/24:0) (m/z 866.6690) Accumulation in the Viable Epidermis of GBA1 KI Mice.

Importantly, this accumulation was selective. The levels of another representative sphingolipid, SM(d18:1/16:0) (m/z 725.5582), and a short-chain glucosylceramide, GlcCer(18:1/12:0) (m/z 666.4847), did not differ significantly between the Hom and WT groups (see Figure 7E-H). The MALDI ion images confirmed that the increased signals for GlcCer(18:1/24:0) and SHexCer(t33:1) were specifically localized to the VE layer and, in some cases, concentrated around sebaceous glands. Together, these findings demonstrate that GCase deficiency leads to a selective and spatially confined dysregulation of glycosphingolipid metabolism in the skin.

4. Discussion

In this study, we employed MALDI-mass spectrometry imaging to conduct the first spatially-resolved investigation of sphingolipid metabolism across the brain-gut-skin axis in a GBA1 D409V KI mouse model of early-stage PD. Our findings move beyond

traditional bulk lipidomics by revealing that GCase deficiency induces not a uniform systemic change, but rather a cascade of early, highly localized, and tissue-specific metabolic dysregulations. We demonstrate GlcCer and GM1 ganglioside accumulation in the CPu of homozygous mice, a progressive accumulation of GlcCer along the gastrointestinal tract peaking in the colon, and a selective enrichment of glycosphingolipids in the viable epidermis of the skin. These spatially-anchored findings provide novel insights into the preclinical pathophysiology of GBA-associated parkinsonism and highlight specific anatomical sites for future biomarker discovery.

In the brain, the observed accumulation of GlcCer species in the CPu of homozygous mice relative to heterozygotes is consistent with a gene-dose-dependent impairment of GCase function, confirming the direct biochemical consequence of the GBA1 mutation [25]. The specific localization of this substrate buildup within the CPu, a core component of the nigrostriatal circuit that degenerates in PD, underscores the regional vulnerability of the dopamine system to GCase-linked metabolic stress. Our spatially-resolved data stand in contrast to some studies on post-mortem human PD-GBA brain tissue, which did not find a significant increase in total GlcCer levels [29]. This discrepancy may arise from critical differences in disease stage and methodology. Our early-stage model captures initial biochemical insults prior to significant neurodegeneration, whereas end-stage human tissue reflects decades of pathology and potential compensatory mechanisms. Furthermore, the homogenization used in bulk analysis may dilute focal accumulations like those we observed in the CPu, potentially masking significant localized changes.

Perhaps the most unexpected finding in the brain was the relative increase in GM1 ganglioside in homozygous mice. This observation appears to contradict numerous reports linking GM1 deficiency to neuronal vulnerability and PD pathogenesis in both patients and toxin-induced models [30,31]. However, this paradoxical increase may represent a complex, stage-dependent adaptive response. In the context of severe GCase deficiency, the elevated GM1 could be a compensatory mechanism aimed at protecting neurons from the escalating toxicity of GlcCer and α-synuclein aggregates [12]. Alternatively, a profound enzymatic block at GCase could force a metabolic rerouting of upstream substrates toward complex ganglioside synthesis. It is crucial, however, to acknowledge a key limitation of our brain analysis. The absence of an anatomically matched wild-type control due to Bregma level disparity. Therefore, we cannot determine the absolute change in GM1 levels relative to a healthy baseline. The observed increase is relative to the heterozygous state and may still represent an overall pathological deviation. This highlights the necessity for future studies incorporating spatial internal standards and precise anatomical matching to enable semi-quantitative analysis.

Moving to the periphery, our analysis of the gastrointestinal tract revealed that the metabolic impact of GCase deficiency is not uniform. The progressive accumulation of GlcCer(d18:1/18:0) along the intestinal axis, culminating in a dramatic increase in the colonic mucosa, points to the distal gut as a site of exceptional metabolic vulnerability. This distal enrichment is biologically plausible, as the colon is known to have lower intrinsic lysosomal enzyme activity and greater exposure to complex sphingolipids from diet and the microbiome compared to the proximal intestine [32,33]. This may render the colon less able to compensate for impaired GCase function, leading to exacerbated substrate accumulation. Pathophysiologically, this is highly relevant, as the colon is considered a potential initiation site for α-synuclein pathology in PD, and patient biopsies have confirmed early pathology in the colonic submucosa [34]. Our layer-resolved imaging, which localizes the most significant GlcCer buildup to the colonic mucosa in the homozygous model, provides a novel molecular link between GCase dysfunction and the known anatomical susceptibility of the colon, suggesting that lipid dysregulation may contribute to the earliest gastrointestinal manifestations of PD.

The skin, as a readily accessible peripheral tissue, mirrored the systemic metabolic disturbance. We observed a significant and selective accumulation of long-chain GlcCer(18:1/24:0) and a putative sulfated hexosylceramide within the viable epidermis of

homozygous mice. This finding is consistent with reports from Gaucher disease models showing cutaneous GlcCer accumulation and subsequent skin barrier defects [18]. While studies in PD patients without GBA1 mutations have reported normal GCase activity in dermal fibroblasts, our model represents a primary, genetically-defined GCase deficiency. The lipid accumulation we observe is the direct downstream consequence of this deficiency. Biologically, since GlcCer in the VE is the precursor for ceramides that form the protective stratum corneum barrier, its accumulation suggests impaired lipid processing that could compromise skin barrier integrity. While the absence of high-quality negative-mode skin data limited our analysis of other key lipids, and the identification of SHexCer remains putative without structural validation, these findings are significant. They spatially localize a specific molecular alteration to an accessible tissue layer, positioning epidermal GlcCer as a promising candidate for a non-invasive biomarker of GCase-related dyslipidemia.

This study has several limitations that should be addressed in future work. The small sample size (n=2 per group) limits statistical power, and the findings warrant validation in larger cohorts. The aforementioned Bregma mismatch in brain sections prevented a complete analysis across all genotypes. Furthermore, the use of only male mice at a single, early time point means that potential sex-dependent differences and the temporal evolution of these lipid changes remain to be explored. Finally, while powerful for discovery, MALDI-MSI-based lipid identification without on-tissue MS/MS remains tentative. Future research should build upon this work by incorporating larger, sex-balanced cohorts and longitudinal designs. Implementing advanced imaging techniques such as parallel reaction monitoring will be crucial for the definitive structural validation and semi-quantification of the candidate lipid biomarkers identified here.

5. Conclusion

In conclusion, by applying MALDI-mass spectrometry imaging to a preclinical model of GBA-associated Parkinson's disease, we have generated a spatially-resolved map of early sphingolipid dysregulation across the brain, gut, and skin. Our results demonstrate that GCase deficiency triggers localized, tissue-specific metabolic alterations, including GlcCer and GM1 accumulation in the CPu, a progressive buildup of GlcCer in the intestinal tract that is most severe in the colonic mucosa, and a selective enrichment of glycosphingolipids in the viable epidermis. These findings support the hypothesis that a systemic enzymatic defect leads to a mosaic of localized pathologies and establish MALDI-MSI as a powerful framework for anatomically-anchored lipidomics. This work not only provides novel mechanistic insights into the earliest stages of GBA-parkinsonism but also identifies the colonic mucosa and epidermis as key vulnerable sites and potential sources of accessible biomarkers, warranting targeted validation in future studies.

References

1. E. Tolosa, A. Garrido, S. W. Scholz, and W. Poewe, "Challenges in the diagnosis of Parkinson's disease," *The Lancet Neurology*, vol. 20, no. 5, pp. 385-397, 2021.
2. E. R. Dorsey, T. Sherer, M. S. Okun, and B. R. Bloem, "The emerging evidence of the Parkinson pandemic," *Journal of Parkinson's disease*, vol. 8, no. s1, pp. S3-S8, 2018. doi: 10.3233/jpd-181474
3. M. T. Hayes, "Parkinson's disease and parkinsonism," *The American journal of medicine*, vol. 132, no. 7, pp. 802-807, 2019.
4. R. F. Pfeiffer, "Non-motor symptoms in Parkinson's disease," *Parkinsonism & related disorders*, vol. 22, pp. S119-S122, 2016.
5. B. R. Bloem, M. S. Okun, and C. Klein, "Parkinson's disease," *The Lancet*, vol. 397, no. 10291, pp. 2284-2303, 2021.
6. Y. E. Huh, T. Usnich, C. R. Scherzer, C. Klein, and S. J. Chung, "GBA1 variants and Parkinson's disease: paving the way for targeted therapy," *Journal of Movement Disorders*, vol. 16, no. 3, p. 261, 2023.
7. E. Sidransky, M. A. Nalls, J. O. Aasly, J. Aharon-Peretz, G. Annesi, E. R. Barbosa, and S. G. Ziegler, "Multicenter analysis of glucocerebrosidase mutations in Parkinson's disease," *New England Journal of Medicine*, vol. 361, no. 17, pp. 1651-1661, 2009.
8. E. Hertz, Y. Chen, and E. Sidransky, "Gaucher disease provides a unique window into Parkinson disease pathogenesis," *Nature Reviews Neurology*, vol. 20, no. 9, pp. 526-540, 2024. doi: 10.1038/s41582-024-00999-z

9. B. Ogretmen, "Sphingolipid metabolism in cancer signalling and therapy," *Nature Reviews Cancer*, vol. 18, no. 1, pp. 33-50, 2018. doi: 10.1038/nrc.2017.96
10. J. A. Motyl, J. B. Strosznajder, A. Wencel, and R. P. Strosznajder, "Recent insights into the interplay of alpha-synuclein and sphingolipid signaling in Parkinson's disease," *International Journal of Molecular Sciences*, vol. 22, no. 12, p. 6277, 2021. doi: 10.3390/ijms22126277
11. A. Kuo, and T. Hla, "Regulation of cellular and systemic sphingolipid homeostasis," *Nature Reviews Molecular Cell Biology*, vol. 25, no. 10, pp. 802-821, 2024. doi: 10.1038/s41580-024-00742-y
12. E. Aflaki, W. Westbroek, and E. Sidransky, "The complicated relationship between Gaucher disease and parkinsonism: insights from a rare disease," *Neuron*, vol. 93, no. 4, pp. 737-746, 2017. doi: 10.1016/j.neuron.2017.01.018
13. A. W. Beger, B. Dudzik, R. L. Woltjer, and P. L. Wood, "Human brain lipidomics: Pilot analysis of the basal ganglia sphingolipidome in Parkinson's disease and Lewy body disease," *Metabolites*, vol. 12, no. 2, p. 187, 2022. doi: 10.3390/metabo12020187
14. R. Yang, C. He, P. Zhang, Y. Li, S. Rong, X. Chen, and Y. Zhang, "Plasma sphingolipids, dopaminergic degeneration and clinical progression in idiopathic Parkinson's disease," *Parkinsonism & Related Disorders*, vol. 126, p. 107071, 2024. doi: 10.1016/j.parkreldis.2024.107071
15. X. Zhang, H. Wu, B. Tang, and J. Guo, "Clinical, mechanistic, biomarker, and therapeutic advances in GBA1-associated Parkinson's disease," *Translational Neurodegeneration*, vol. 13, no. 1, p. 48, 2024. doi: 10.1186/s40035-024-00437-6
16. H. Braak, K. Del Tredici, U. Rüb, R. A. De Vos, E. N. J. Steur, and E. Braak, "Staging of brain pathology related to sporadic Parkinson's disease," *Neurobiology of aging*, vol. 24, no. 2, pp. 197-211, 2003.
17. Z. A. Al-Azzawi, S. Arfaie, and Z. Gan-Or, "GBA1 and the immune system: A potential role in Parkinson's disease?," *Journal of Parkinson's Disease*, vol. 12, no. s1, pp. S53-S64, 2022. doi: 10.3233/jpd-223423
18. J. M. den Heijer, V. C. Cullen, D. R. Pereira, Y. Yavuz, M. L. de Kam, H. W. Grievink, and G. J. Groeneveld, "A biomarker study in patients with GBA1Parkinson's disease and healthy controls," *Movement Disorders*, vol. 38, no. 5, pp. 783-795, 2023.
19. L. M. Collins, J. Drouin-Ouellet, W. L. Kuan, T. Cox, and R. A. Barker, "Dermal fibroblasts from patients with Parkinson's disease have normal GCase activity and autophagy compared to patients with PD and GBA mutations," *F1000Research*, vol. 6, p. 1751, 2018.
20. E. Sinclair, D. K. Trivedi, D. Sarkar, C. Walton-Doyle, J. Milne, T. Kunath, and P. Barran, "Metabolomics of sebum reveals lipid dysregulation in Parkinson's disease," *Nature communications*, vol. 12, no. 1, p. 1592, 2021. doi: 10.1038/s41467-021-21669-4
21. M. Aichler, and A. Walch, "MALDI Imaging mass spectrometry: current frontiers and perspectives in pathology research and practice," *Laboratory investigation*, vol. 95, no. 4, pp. 422-431, 2015. doi: 10.1038/labinvest.2014.156
22. B. Enthaler, M. Trusch, M. Fischer, C. Rapp, J. K. Pruns, and J. P. Vietzke, "MALDI imaging in human skin tissue sections: focus on various matrices and enzymes," *Analytical and bioanalytical chemistry*, vol. 405, no. 4, pp. 1159-1170, 2013.
23. Q. Zhang, Y. Li, P. Sui, X. H. Sun, Y. Gao, and C. Y. Wang, "MALDI mass spectrometry imaging discloses the decline of sulfoglycosphingolipid and glycerophosphoinositol species in the brain regions related to cognition in a mouse model of Alzheimer's disease," *Talanta*, vol. 266, p. 125022, 2024.
24. T. Pingale, and G. L. Gupta, "Classic and evolving animal models in Parkinson's disease," *Pharmacology Biochemistry and Behavior*, vol. 199, p. 173060, 2020. doi: 10.1016/j.pbb.2020.173060
25. N. K. Polinski, T. N. Martinez, A. Gorodinsky, R. Gareus, M. Sasner, M. Herberth, and K. D. Dave, "Decreased glucocerebrosidase activity and substrate accumulation of glycosphingolipids in a novel GBA1 D409V knock-in mouse model," *PloS one*, vol. 16, no. 6, p. e0252325, 2021. doi: 10.1371/journal.pone.0252325
26. W. H. Jordan, "Book review: the rat brain in stereotaxic coordinates," 2006. doi: 10.1354/vp.43-1-86-a
27. E. Fahy, M. Sud, D. Cotter, and S. Subramaniam, "LIPID MAPS online tools for lipid research," *Nucleic acids research*, vol. 35, no. suppl_2, pp. W606-W612, 2007.
28. Z. Pang, J. Chong, G. Zhou, D. A. de Lima Morais, L. Chang, M. Barrette, and J. Xia, "MetaboAnalyst 5," *0: narrowing the gap between raw spectra and functional insights. Nucleic acids research*, vol. 49, no. W1, pp. W388-W396, 2021.
29. S. Blumenreich, T. Nehushtan, O. B. Barav, J. T. Saville, T. Dingjan, J. Hardy, and A. H. Futerman, "Elevation of gangliosides in four brain regions from Parkinson's disease patients with a GBA mutation," *npj Parkinson's Disease*, vol. 8, no. 1, p. 99, 2022. doi: 10.1038/s41531-022-00363-2
30. G. Wu, Z. H. Lu, N. Kulkarni, and R. W. Ledeen, "Deficiency of ganglioside GM1 correlates with Parkinson's disease in mice and humans," *Journal of neuroscience research*, vol. 90, no. 10, pp. 1997-2008, 2012.
31. S. Chowdhury, and R. Ledeen, "The key role of GM1 ganglioside in Parkinson's disease," *Biomolecules*, vol. 12, no. 2, p. 173, 2022. doi: 10.3390/biom12020173
32. T. Sugawara, T. Tsuduki, S. Yano, M. Hirose, J. Duan, K. Aida, and T. Hirata, "Intestinal absorption of dietary maize glucosylceramide in lymphatic duct cannulated rats," *Journal of lipid research*, vol. 51, no. 7, pp. 1761-1769, 2010. doi: 10.1194/jlr.m002204
33. R. D. Duan, "Alkaline sphingomyelinase: an old enzyme with novel implications," *Biochimica et Biophysica Acta (BBA)-Molecular and Cell Biology of Lipids*, vol. 1761, no. 3, pp. 281-291, 2006.

34. K. M. Shannon, A. Keshavarzian, E. Mutlu, H. B. Dodiya, D. Daian, J. A. Jaglin, and J. H. Kordower, "Alphasynuclein in colonic submucosa in early untreated Parkinson's disease," *Movement Disorders*, vol. 27, no. 6, pp. 709-715, 2012. doi: 10.1002/mds.23838